Chinese Chemical Letters 36 (2025) 110391

Contents lists available at ScienceDirect

Chinese Chemical Letters

journal homepage: www.elsevier.com/locate/cclet

Mechanical-durable and humidity-resistant dry-processed halide solid-state electrolyte films for all-solid-state battery

Mufan Cao[a,1], Long Pan[a,1,*], Yaping Wang[a], Xianwei Sui[b], Xiong Xiong Liu[a], Shengfa Feng[a], Pengcheng Yuan[a], Min Gao[a], Jiacheng Liu[c], Song-Zhu Kure-Chu[c], Takehiko Hihara[c], Yang Zhou[d,*], Zheng-Ming Sun[a,*]

[a] Key Laboratory of Advanced Metallic Materials of Jiangsu Province, School of Materials Science and Engineering, Southeast University, Nanjing 211189, China
[b] Daikin Fluorochemicals (China) Co., Ltd., Shenzhen 518129, China
[c] Department of Materials Function and Design, Nagoya Institute of Technology, Gokiso-cho, Showa-ku, Nagoya, Aichi 466-8555, Japan
[d] Jiangsu Key Laboratory of Construction Materials, School of Materials Science and Engineering, Southeast University, Nanjing 211189, China

ARTICLE INFO

Article history:
Received 2 June 2024
Revised 2 August 2024
Accepted 29 August 2024
Available online 31 August 2024

Keywords:
Halide solid-state electrolytes
Dry-process
Humidity resistance
Mechanical durability
All solid-state battery

ABSTRACT

Halide solid-state electrolytes (HSSEs) with excellent ionic conductivity and high voltage stability are promising for all-solid-state Li-ion batteries (ASSLBs). However, they suffer from poor processability, mechanical durability and humidity stability, hindering their large-scale applications. Here, we introduce a dry-processing fibrillation strategy using hydrophobic polytetrafluoroethylene (PTFE) binder to encapsulate Li_3InCl_6 (LIC) particles (the most representative HSSE). By manipulating the fibrillating process, only 0.5 wt% PTFE is sufficient to prepare free-standing LIC-PTFE (LIC-P) HSSEs. Additionally, LIC-P demonstrates excellent mechanical durability and humidity resistance. They can maintain their shapes after being exposed to humid atmosphere for 30 min, meanwhile still exhibit high ionic conductivity of > 0.2 mS/cm at 25 °C. Consequently, the LIC-P-based ASSLBs deliver a high specific capacity of 126.6 mAh/g at 0.1 C and long cyclability of 200 cycles at 0.2 C. More importantly, the ASSLBs using moisture-exposed LIC-P can still operate properly by exhibiting a high capacity-retention of 87.7% after 100 cycles under 0.2 C. Furthermore, for the first time, we unravel the LIC interfacial morphology evolution upon cycling because the good mechanical durability enables a facile separation of LIC-P from ASSLBs after testing.

Li-ion batteries (LIBs) are the most important power sources for consumer electronics and electric vehicles. However, the safety issues of LIBs still concern owing to the flammable liquid electrolytes and organic separators, and the energy density of LIBs has almost reached theoretical limits [1,2]. All-solid-state Li-ion batteries (ASSLBs) are therefore developed by replacing liquid electrolyte and organic separator with nonflammable solid-state electrolytes (SSEs), thus both energy density and safety are enhanced [3,4]. The past decade has witnessed the development of various SSEs, such as polymers, oxides, sulfides and halides [5-12]. Among them, halide SSEs (HSSEs) display 1 mS/cm-level room-temperature (RT) ionic conductivities and show good compatibilities towards high-voltage cathode materials, enabling high-energy-density ASSLBs [13-18].

However, HSSEs suffer from moisture instability and poor formability. Firstly, HSSEs are highly hydroscopic and deteriorate quickly when exposed to ambient air, which limit their applications [19,20]. To date, two methods have been investigated to improve the moisture stability of HSSEs: Introducing other moisture-stable elements and coating the surface *via* powder atomic layer deposition [19,21,22]. However, both methods require extra complexity and cost for production, and the electrochemical performances of modified HSSEs in ASSLBs are hardly mentioned. Secondly, as a powder-type inorganic SSE, the stiffness and brittleness of HSSEs particles lead to poor adhesion and formability [23]. To address this common issue of inorganic SSEs, polymer binders are often introduced to form free-standing composite SSE films *via* tape casting, but solvents are detrimental to HSSEs and lead to reduced ionic conductivity [24]. Therefore, developing a viable method to fabricate mechanically durable HSSE films with im-

* Corresponding authors.
E-mail addresses: panlong@seu.edu.cn (L. Pan), tomaszy@seu.edu.cn (Y. Zhou), zmsun@seu.edu.cn (Z.-M. Sun).
[1] These authors contributed equally to this work.

https://doi.org/10.1016/j.cclet.2024.110391
1001-8417/

proved humidity resistance would be crucial for ASSLB commercialization.

Polytetrafluoroethylene (PTFE) is a type of deformable organic binders which can form fibers under shear force [25,26]. With very little amount of PTFE added (usually < 2 wt%), the fibrillated PTFE can interweave the particles together and from free-standing films. This dry-processing method has been widely reported in high mass loading electrodes and sulfide SSEs (SSSEs), but hardly used in HSSEs [27,28]. Moreover, PTFE is also known as a widely-used hydrophobic coating material with a water contact angle of ~120° [29]. Therefore, the introduction of fibrillated PTFE into HSSEs may improve the mechanical processability and humidity stability of the obtained film at the same time, which has not been investigated to date.

Herein, we propose a dry-processing strategy to fabricate HSSEs-based film using Li_3InCl_6 (LIC) as Li^+ conductor and powder-type PTFE as polymer binder, which could address the poor mechanical durability and humidity instability of LIC simultaneously. Two fabrication parameters, PTFE weight ratio and fibrillation temperature, are optimized during fabricating LIC-*x*%PTFE film (denoted as LIC-*x*P, where *x* refers to the weight ratio of PTFE in the films), and the ideal parameters are confirmed by observing PTFE morphology *via* scanning electron microscopy (SEM). Owing to the hydrophilicity of PTFE, LIC-*x*P exhibits exceptional mechanical durability for 30 min with ionic conductivity maintains > 0.2 mS/cm in open environment. The ASSLBs using LIC-*x*P display specific discharge capacity of 126.6 mAh/g and initial Coulombic efficiency (CE) of 85.3% at 0.1 C. The long cycling stability (200 cycles, 0.2 C) of LIC-*x*P surpasses most reported works that combines LIC with polymer binders and applies lithium nickel cobalt manganese oxide (NCM) cathodes (typically below 50 cycles) [21,24,30,31]. Moreover, the ASSLBs using humidity-exposed LIC-*x*P exhibit specific discharge capacity of 69.5 mAh/g with cycling stability of 100 cycles at 0.2 C. Finally, owning to the good formability and durability enabled by PTFE, the surfaces of cycled LIC-*x*P are separated and observed by SEM, and the evidence of reaction between LIC and Li_6PS_5Cl (LPSC) is validated.

To prepare LIC-*x*P, LIC (Shenzhen Kejing Star Technology Company) with various PTFE (F-106C, Daikin Fluorochemicals (China) Co., Ltd., Shenzhen) ratios (*i.e.*, 0.2, 0.5, 1, and 2 wt%) were uniformly mixed by a shaker, followed by shear-mixing in a mortar until a dough was formed (Fig. 1a). The dough was then put in a plastic bag and calendared 15 times by a calendar machine at different temperatures (*i.e.*, 25 and 100 °C), during which the roller gap was gradually declined from 1000 μm to 300 μm. Note that the thickness of the plastic bag is ~130 μm as measured, the actual thickness of the LIC-*x*P film was ~170 μm (Fig. S1 in Supporting information). For every calendar loop, the SSE film was calendared, detached and folded in half, then calendared again, obtaining freestanding LIC-*x*P films (except the case of LIC-0.2P, Fig. S1 in Supporting information). Finally, LIC-*x*P films were punched into pieces with diameter of 10 mm, followed by pressing at the pressure of 4 tons for 5 min, resulting in relatively rigid pellets for further characterizations and tests. The pure LIC pellets were prepared by pressing LIC particles without PTFE using the same parameters (4 tons for 5 min). All procedures were performed inside an Ar-filled glovebox.

To test the ionic conductivity of LIC-*x*P, the samples were placed in a 10 mm poly(ether-ether-ketone) (PEEK) die and pressed at 4 t for 5 min with stainless plungers, which was subsequently tested under room temperature using a Bio-Logic SP150 electrochemical workstation by the electrochemical impedance spectroscopy (EIS) method (frequency range: 500 kHz to 10 mHz). For the ionic conductivity measurements of moisture-exposed LIC-0.5P, the pellets were exposed in ambient air for desired time (from 1 min to 30 min), followed by removing surface water droplets using dust-free paper.

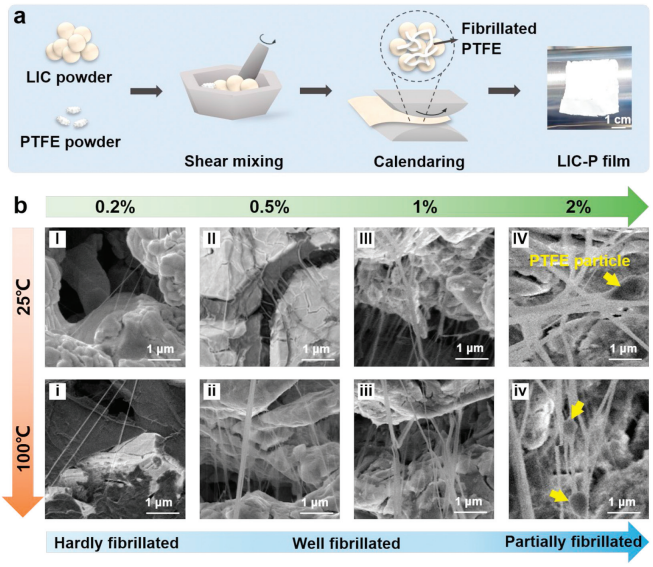

Fig. 1. Preparation and morphological information of LIC-*x*P films. (a) Schematic of dry-processing fabrication of LIC-*x*P films. (b) SEM images of LIC-*x*P films fabricated with different PTFE weight ratios and calendaring temperatures. The yellow arrows in b-IV and iv show the PTFE particles that are not fibrillated.

For the assembly of ASSLBs, cathode was prepared by mixing NCM811 (Ningbo Ronbay New Energy Technology Co., Ltd.), LIC and VGCF (Showa Denko) with a weight ratio of 70:30:0.5 in a mortar and hand grounding for 30 min, obtaining homogeneous powder. Li-In anode was prepared by putting a Li foil (6 mm diameter, 0.1 mm thickness) between two pieces of In foils (9 mm diameter, 0.1 mm thickness), then placed on a Cu foam (10 mm diameter, 0.2 mm thickness) together in a 10 mm diameter die and pressed at 4 t for 15 min. To assemble ASSLBs, 50 mg of LPSC (Shenzhen Kejing Star Technology Company) was firstly placed and evenly spread into a 10 mm PEEK die and pressed under 4 tons for 5 min. Afterward, a piece of LIC-0.5P pellet was placed above LPSC and pressed similarly. Subsequently, 8 mg of cathode powder was placed above LIC-0.5P pellet and pressed similarly. Finally, a piece of Li-In anode was placed on the other side of LPSC, followed by pressing the whole ASSLB at 1 ton for 15 min. All galvanostatic charge/discharge tests were performed on a Neware CT-4008 tester at the voltage range of 1.80-3.65 V (*vs.* Li^+/Li-In) at 45 °C. For the ASSLBs using moisture-exposed LIC-0.5P, all procedures were the same, except that the LIC-0.5P was exposed in ambient air for 1 min and then dried overnight inside an Ar-filled glovebox at room temperature. For the ASSLBs using moisture-exposed LIC, the LIC pellets were similarly processed (*i.e.*, exposure and drying). However, the obtained LIC pellets were subsequently ground into powder, followed by mixing with 0.5 wt% PTFE, then processed in the same way LIC-0.5P film was formed.

For the characterization of the materials, SEM images were acquired using a Nova Nano SEM450 (field emission) or a FEI Sirion scanning electron microscope. X-ray diffraction (XRD) patterns were recorded using a Haoyuan DX-2700BH diffractometer. During XRD tests, all samples were covered by a thin mylar film (Premierlabsupply, TF-115) to isolate open environment. The wettability test was performed using a DataPhysics OCA25LHT-SV contact angle measuring apparatus.

To understand the influence of weight ratios and calendaring temperatures on the fibrillation of PTFE, SEM is applied to characterize the morphologies of PTFE fibers. Fig. 1b, I-IV show the SEM

images of LIC-*x*P films with different PTFE weight ratios (all calendared at 25 °C). In the case of LIC-0.2P@25 °C, the film is poorly formed and not durable (Fig. S1 in Supporting information), which cannot be used for further electrochemical tests. The poor formability and mechanical durability are attributed to the formation of few and slim PTFE fibers (Fig. 1b-I). When the PTFE ratio is increased to 0.5 wt%, more and thicker PTFE fibers are observed (Fig. 1b-II), resulting in foldable LIC-0.5P@25 °C film with much better formability and durability (Fig. S2 in Supporting information). In addition, the LIC-0.5P@25 °C film also delivers high RT ionic conductivity of 0.6 mS/cm (Fig. S3 in Supporting information). However, with the PTFE ratio further increases (*e.g.*, 1 and 2 wt%), the PTFE fibers become uneven, and some PTFE particles are not fibrillated (Fig. 1b-III, IV). What is worse, the RT ionic conductivity quickly declined to 0.4 and 0.1 mS/cm at the PTFE ratio of 1 and 2 wt%, respectively (Fig. S3). The decrease of ionic conductivity is caused by the increased binder volume which hinders interparticle contacts [28,32]. Therefore, PTFE ratio of 0.5 wt% is preferred for further electrochemical tests because of its high ionic conductivity as well as good formability and mechanical durability.

The effect of temperature on PTFE fibrillation is also investigated by changing the calendaring temperature from 25 °C to 100 °C (Fig. 1b, i-iv). At PTFE ratio of 0.2 wt%, more fibers are witnessed at 100 °C, but still too few and too fine in comparison with the films formed at higher PTFE weight ratio. At PTFE ratio of above 0.5 wt%, the PTFE fibers are also thicker and better cross-linked at 100 °C. This trend is attributed to the temperature-dependent changing behavior of PTFE. With the rising of calendaring temperature, the movement of the PTFE polymer chain segment become faster, thus the degree of PTFE fibrillation is increased [28]. Note that the rising calendaring temperature can also improve the Li^+ conductivity of LIC-*x*P films. For instance, the RT ionic conductivity of LIC-0.5P@100 °C films increased to 0.7 mS/cm (Fig. S4 in Supporting information), which is almost 1.2 times than LIC-0.5P@25 °C (0.6 mS/cm). The enhancement of Li^+ conductivity may be attributed to the reduction of hopping energy within the grains [14].

To summarize our results up to this point, the formability and ionic conductivity can be regulated by taming the PTFE weight ratio and fibrillation temperature. The higher PTFE weight ratio results in better formability. The ionic conductivity can be enhanced by optimizing PTFE weight ratio (0.5 wt% in our case) and improving fibrillation temperature (100 °C in our case). Since the XRD patterns of LIC before and after combined with PTFE show little difference, the minor addition of PTFE into LIC has hardly changed the crystallographic structure of LIC (Fig. S5 in Supporting information). Therefore, LIC-*x*P film fabricated at 0.5 wt% PTFE weight ratio and 100 °C (denoted as LIC-0.5P) is selected for further investigation for its high ionic conductivity and satisfying formability.

To compare the mechanical durability and humidity resistance, pure LIC and LIC-0.5P are exposed in open environment (RT, relative humidity = 86%) for 30 min, and the corresponding morphology stability are evaluated. Fig. 2a shows the appearance changes of pure LIC and LIC-0.5P pellets after exposing for different times. For pure LIC, the pellet wrinkles and the edge coarsen after only 1-min exposure. As the exposure time increases, LIC pellet swells quickly, and cracks appear after 5-min exposure. What is worse, the pellet cannot maintain its shape after 10 min and thoroughly broken after 15 min. These results confirm the extremely poor mechanical durability and humidity resistance of pure LIC pellet. In contrast, the LIC-0.5P pellet can generally maintain its shape after 30-min exposure without any obvious cracks. Surprisingly, an increasing number of water droplets are observed on and around the LIC-0.5P pellet as the exposure time increases, indicating that the LIC-0.5P pellet are highly hydrophobic and almost does not absorb water. However, XRD result confirmed that a small amount of LIC hydrate still appeared in LIC-0.5P after 1 min' exposure to air (Fig. S6 in Supporting information). These findings firmly demonstrate that wrapping PTFE fibers around LIC particles can significantly improve the mechanical durability and humidity resistance of LIC.

The mechanical durability and humidity resistance of LIC-0.5P can be attributed to the high hydrophobicity of pure PTFE, as demonstrated by contact angle and mass change characterizations. Fig. 2b validates the super-hydrophilicity of pure LIC pellet, in which it shows an extremely small contact angle of 5° with water droplet. In contrast, LIC-0.5P pellet exhibits a large contact angle of 82° (Fig. 2c), implying its good hydrophobicity impeding water infiltration. Fig. 2d presents the relationship between pellet mass and exposure time. After exposing for 30 min, the mass of pure LIC pellet increases by 11%, which is over 2 times than that of LIC-0.5P pellet (5%). This result indicates that pure LIC has a much larger tendency to absorb water from the surrounding atmosphere than LIC-0.5P. In other words, introducing fibrillated PTFE can efficiently reduce the hygroscopicity of pure LIC, resulting in impressive mechanical durability and humidity resistance. Benefiting from these merits, the RT ionic conductivity of LIC-0.5P pellet can be mostly remained, with the value change from 0.7 mS/cm to 0.2 mS/cm after 30 min exposure, endowing LIC-0.5P with application potentials in open environments (Fig. 2e). Note that the RT ionic conductivity of pure LIC after exposure cannot be tested because the pellets are destroyed.

Based on the results above, we propose a mechanism for the enhanced mechanical durability and humility resistance of LIC by introducing fibrillated PTFE (Fig. 2f). Upon air exposure, pure LIC absorbs moisture from the surrounding atmosphere and is gradually hydrated into LIC·$2H_2O$ with volume expansion [19,20]. Finally, the LIC pellets break because there are no strong interactions between LIC particles to secure the pellet volume and shape. In the case of LIC-0.5P, conversely, the hydrophobic PTFE fibers form an intertangled network around LIC particles, which not only prevents LIC from absorbing water, but also ties LIC particles together to avoid deformation.

To evaluate the electrochemical performance of LIC-0.5P, ASSLBs were assembled using NCM811 and Li-In alloy as cathode and anode, respectively (Fig. 3a). Note that a 150 μm thick layer of LPSC is sandwiched between LIC-0.5P and Li-In anode to prevent the reaction between LIC and Li (Fig. S7 in Supporting information) [33]. The rate performances of LIC-0.5P at different current densities are presented in Fig. 3b. At current densities of 0.1, 0.2, 0.3, 0.5, 1 and 2 C, LIC-0.5P demonstrates reversible specific discharge capacities of 126.6, 115.7, 107.4, 94.3, 73.6 and 41.5 mAh/g, respectively, indicating its good rate capability. When the current densities are gradually restored to 0.1 C (in sequence of 1, 0.5, 0.3, 0.2 and 0.1 C), the specific discharge capacity of LIC-0.5P recovers to 72.6, 92.3, 104.0, 111.0 and 120.1 mAh/g, respectively, suggesting its ability to withstand the rapid transfer of Li^+ ions. To further evaluate the high reversibility of LIC-0.5P, the first three cycles of the galvanostatic charge-discharge curves of LIC-0.5P are displayed in Fig. 3c. At the 1st cycle, LIC-0.5P exhibits high CE of 85.3%, validating its high electrochemical reversibility. Fig. 3d shows the cycling performance of LIC-0.5P. At the current density of 0.2 C, LIC-0.5P can successively charge-discharge for 200 cycles, and maintains 76.0% and 47.4% of its initial specific discharge capacity after 100 and 200 cycles, respectively. It is worth mentioning that the cycle life and capacity retention of LIC-0.5P outperforms most reported works which combine LIC with organic binders and employ NCM cathode materials (Fig. 3f) [21,24,30,31].

To further demonstrate the humidity resistance advantages of LIC-0.5P, both LIC and LIC-0.5P were first exposed to air and subsequently assembled in ASSLBs for cycling tests. As shown in Fig. 3e, the exposed pure-LIC-based ASSLB delivers an initial specific dis-

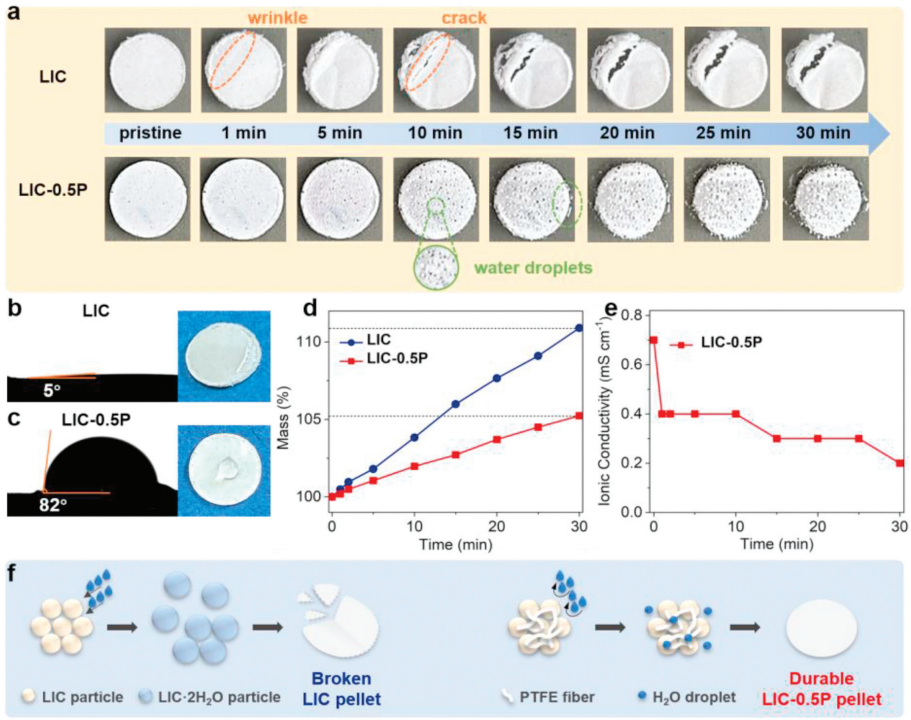

Fig. 2. Mechanical durability and humidity resistance evaluation. (a) Photographs of pure LIC and LIC-0.5P pellets before and after exposing in open environment for different times. (b, c) Images of contact angles of water droplets on pure LIC and LIC-0.5P pellets. (d) Mass *vs.* exposure time curves of pure LIC and LIC-0.5P pellets (ordinate normalized by mass). (e) RT ionic conductivity *vs.* exposure time curve of LIC-0.5P pellet. (f) Schematic of fibrillated PTFE preventing LIC from absorbing water and broken.

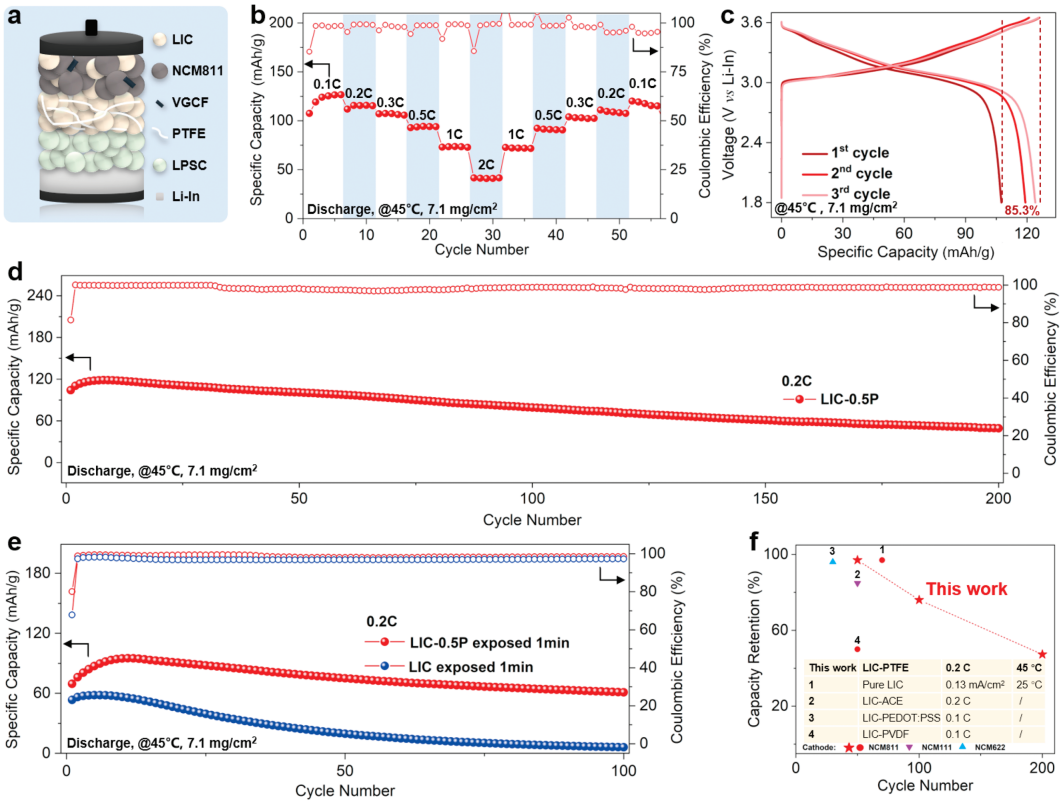

Fig. 3. Electrochemical performance of ASSLBs. (a) Schematic of the LIC-0.5P-based ASSLB using NCM811 as cathode and Li-In alloy as anode. (b) Rate capability of LIC-0.5P-based ASSLBs at various current densities. (c) The first three galvanostatic charge/discharge profiles of LIC-0.5P-based ASSLBs at the current density of 0.1 C. (d) Cycling performance of LIC-0.5P-based ASSLBs at the current density of 0.2 C. (e) Cycling performances of exposed pure-LIC-based and exposed LIC-0.5P-based ASSLBs at the current density of 0.2 C. All ASSLBs were tested at 45 °C. (f) Cycling life, capacity retention and testing temperature compared with reported works. Note that the testing temperatures of reference 2-4 are not mentioned.

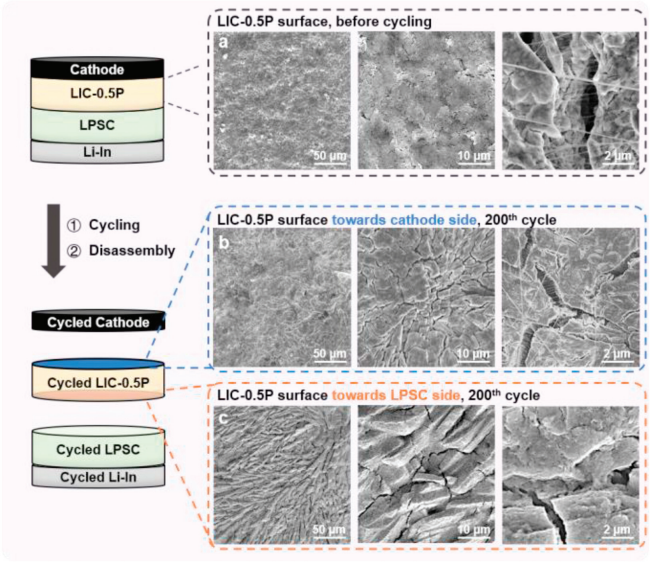

Fig. 4. Postmortem examination of cycled LIC-0.5P. SEM images of (a) LIC-0.5P surfaces before cycling and cycled LIC-0.5P surfaces towards (b) cathode side and (c) LPSC side, respectively, at the 200th cycle.

charge capacity of 53.4 mAh/g, which quickly declines to almost 0 mAh/g after 100 cycles. This result indicates that the hydrated LIC can severely deteriorate the cycling stability of ASSLBs. In contrast, the exposed LIC-0.5P-based ASSLB exhibits initial specific discharge capacity of 69.5 mAh/g, which can be largely maintained after 100 cycles. These findings once again validate that introducing fibrillated PTFE can prevent LIC from absorbing moisture from humid air, representing a significant step forward for the practical applications of LIC-based SSEs.

However, the rise in impedance of the ASSLB before and after cycling leads to concern of the electro-chemical stability of LIC-0.5P inside ASSLBs (Fig. S8 in Supporting information). TEM were applied to comparatively study the evolutions of interfaces during cycling (Fig. 4). Taken the advantage of the mechanical durability of LIC-0.5P, we were able to separate cycled LIC-0.5P from the disassembled ASSLBs (Fig. S9 in Supporting information). To study the evolution of LIC-morphology, the surfaces of cycled LIC-0.5P were observed by SEM. In general, the surface of LIC-0.5P is even before cycling, and LIC particles and PTFE fibers could be clearly observed (Fig. 4a). Note that the minor cracks appeared at the surface might be produced during the preparation of samples. At cathode side, the morphology of cycled LIC-0.5P surface shows little difference (Fig. 4b). The surface is still well-preserved, and the PTFE fibers are still clearly observed. However, the number of cracks increases in comparison with pristine LIC-0.5P, which is most likely caused by the volume change of active cathode materials during cycling [34]. At LPSC side, the cycled LIC-0.5P exhibits an extremely rough surface with mountain-like morphology and deep cracks in Fig. 4c. This result validates the severe interface reaction between LIC and LPSC. Moreover, traces of PTFE fibers are missing after cycling. Since PTFE has been proved unstable at low potential, the PTFE fibers on the surface of LIC-0.5P might have decomposed at the LIC/LPSC interface [35]. However, due to the minor amount of PTFE added (0.5 wt%), it would be impractical to quantify the specific reaction of PTFE decomposition. Although LIC and LPSC has been considered chemically compatible in most cases, previous work has found evidence of the onset of parasitic chemical reactions between LIC and LPSC [36,37]. In this work, we found that the interface of LIC/LPSC might be stable at the beginning, yet interfacial deterioration happened during cycling as the morphology of cycled LIC-0.5P obviously changed. Therefore, we suggest that the reaction between LIC and LPSC could not be ignored in constructing ASSLBs, and the specific reaction mechanism still requires further investigation.

In conclusion, we proposed dry-processed LIC-*x*P films with enhanced mechanical durability and humidity resistance. The degree of PTFE fibrillation is affected by PTFE ratio and fibrillating temperature. While higher temperature leads to higher ionic conductivity, there is a trade-off between PTFE ratio and ionic conductivity. With only 0.5 wt% PTFE added, the high ionic conductivity of LIC is preserved, and the humidity stability of LIC-0.5P film is significantly improved comparing with pure LIC. The LIC-0.5P exhibits exceptional mechanical durability for 30 min with ionic conductivity maintains $>$ 0.2 mS/cm in ambient air. LIC-0.5P exhibits satisfying electrochemical performances, with specific discharge capacity of 126.6 mAh/g at 0.1 C and long cycling stability of 200 cycles at 0.2 C. Moreover, the moisture-exposed LIC-P film exhibits steady charging-discharging of 100 cycles, while moisture-exposed LIC hardly provides any capacity after 50 cycles. Although most previous works have considered the interface between HSSEs and SSSEs as stable, our work provides a different view of the evolution between LIC/LPSC interface. Enabled by the good mechanical durability of LIC-0.5P, the surfaces of cycled LIC-0.5P are separated and we are able to visualize the reaction between LIC and LPSC. Hopefully, our proposed dry-processing approach with enhanced mechanical durability and humidity resistance could be a viable technology that ensures a smooth transition of HSSEs from laboratory research to factory manufacturing.

Declaration of competing interest

The authors declare that they have no known competing financial interests or personal relationships that could have appeared to influence the work reported in this paper.

CRediT authorship contribution statement

Mufan Cao: Writing – original draft, Visualization, Investigation, Formal analysis, Data curation, Conceptualization. **Long Pan:** Writing – review & editing, Visualization, Supervision, Resources, Project administration, Funding acquisition, Conceptualization. **Yaping Wang:** Supervision, Resources, Methodology, Data curation, Conceptualization. **Xianwei Sui:** Resources, Methodology. **Xiong Xiong Liu:** Validation, Investigation. **Shengfa Feng:** Validation, Investigation. **Pengcheng Yuan:** Validation, Investigation. **Min Gao:** Validation, Investigation. **Jiacheng Liu:** Investigation. **Song-Zhu Kure-Chu:** Supervision. **Takehiko Hihara:** Supervision. **Yang Zhou:** Supervision, Resources, Project administration, Funding acquisition. **Zheng-Ming Sun:** Writing – review & editing, Validation, Supervision, Resources, Project administration, Funding acquisition.

Acknowledgments

This work was supported by the 261 Project of MIIT, the National Natural Science Foundation of China (Nos. 52250010, 52201242, U23A20574) and the Young Elite Scientists Sponsorship Program by CAST (No. 2021QNRC001).

Supplementary materials

Supplementary material associated with this article can be found, in the online version, at doi:10.1016/j.cclet.2024.110391.

References

[1] M. Li, J. Lu, Z. Chen, K. Amine, Adv. Mater. 30 (2018) 1800561.
[2] F. Wu, J. Maier, Y. Yu, Chem. Soc. Rev. 49 (2020) 1569–1614.

[3] A. Banerjee, X. Wang, C. Fang, E.A. Wu, Y.S. Meng, Chem. Rev. 120 (2020) 6878–6933.
[4] J. Chen, J. Wu, X. Wang, A.A. Zhou, Z. Yang, Energy Storage Mater. 35 (2021) 70–87.
[5] L. Pan, S. Sun, G. Yu, et al., Chem. Eng. J. 449 (2022) 137682.
[6] G. Yu, Y. Wang, K. Li, et al., Chem. Eng. J. 430 (2022) 132874.
[7] X. Li, J. Liang, J. Luo, et al., Energy Environ. Sci. 12 (2019) 2665–2671.
[8] Y. Jin, Q. He, G. Liu, et al., Adv. Mater. 35 (2023) 2211047.
[9] Z. Zhang, L. Wu, D. Zhou, W. Weng, X. Yao, Nano Lett. 21 (2021) 5233–5239.
[10] Z. Zhang, J. Wang, Y. Jin, et al., Energy Storage Mater. 54 (2023) 845–853.
[11] L. Pan, S. Feng, H. Sun, et al., Small 20 (2024) 2400272.
[12] Y. Wang, P. Yuan, X.X. Liu, et al., Adv. Funct. Mater. 34 (2024) 2405060.
[13] F. Li, X. Cheng, J. Luo, H. Yao, Energy Storage Sci. Technol. 13 (2024) 193–211.
[14] W. Li, J.A. Quirk, M. Li, et al., Adv. Mater. 36 (2023) 2302647.
[15] Y. Gu, K. Yang, H. Yao, et al., Chin. Chem. Lett. 34 (2023) 108047.
[16] S. Chen, C. Yu, C. Wu, et al., Chin. Chem. Lett. 34 (2023) 107544.
[17] H. Zhang, Z. Yu, J. Chen, et al., Chin. Chem. Lett. 34 (2023) 108228.
[18] S. Chen, C. Yu, S. Chen, et al., Chin. Chem. Lett. 33 (2022) 4635–4639.
[19] S. Wang, X. Xu, C. Cui, et al., Adv. Funct. Mater. 32 (2021) 2108805.
[20] X. Li, J. Liang, N. Chen, et al., Angew. Chem. Int. Ed. 58 (2019) 16427–16432.
[21] X. Chen, Z. Jia, H. Lv, et al., J. Power Sources 545 (2022) 231939.
[22] X. Li, J. Liang, K.R. Adair, et al., Nano Lett. 20 (2020) 4384–4392.
[23] S. Wang, Y. Liao, S. Li, et al., Adv Energy Mater. 14 (2023) 2303641.
[24] H. Li, G. Du, H. Liang, et al., J. Alloys Compd. 969 (2023) 172418.
[25] Y. Li, Y. Wu, Z. Wang, et al., Mater. Today 55 (2022) 92–109.
[26] B. Zhao, Y. Lu, B. Yuan, Z. Wang, X. Han, Mater. Lett. 310 (2022) 131463.
[27] W. Yao, M. Chouchane, W. Li, et al., Energy Environ. Sci. 16 (2023) 1620–1630.
[28] D.J. Lee, J. Jang, J.P. Lee, et al., Adv. Funct. Mater. 33 (2023) 2301341.
[29] T. Kamegawa, Y. Shimizu, H. Yamashita, Adv. Mater. 24 (2012) 3697–3700.
[30] E. Nazmutdinova, C. Rosenbach, C. Schmidt, et al., Batter. Supercaps 7 (2024) e202300434.
[31] H.X. Mei, P. Piccardo, G. Carraro, M. Smerieri, R. Spotorno, J. Energy Storage 72 (2023) 108244.
[32] S. Wang, X. Zhang, S. Liu, et al., J. Materiomics 6 (2020) 70–76.
[33] L.M. Riegger, R. Schlem, J. Sann, W.G. Zeier, J. Janek, Angew. Chem. Int. Ed. 60 (2021) 6718–6723.
[34] T. Ma, Z. Wang, D. Wu, et al., Energy Environ. Sci. 16 (2023) 2142–2152.
[35] G. Li, Solid State Ion 90 (1996) 221–225.
[36] C. Rosenbach, F. Walther, J. Ruhl, et al., Adv. Energy Mater. 13 (2022) 2203673.
[37] T. Koç, M. Hallot, E. Quemin, et al., ACS Energy Lett. 7 (2022) 2979–2987.